Korean J. Chem. Eng.
DOI: 10.1007/s11814-018-0063-3

pISSN: 0256-1115
eISSN: 1975-7220

Numerical study on particle deposition in rough channels with large-scale irregular roughness

Wenpeng Hong and Xin Wang†

School of Energy and Power Engineering, Northeast Electric Power University, Jilin 132012, China
(*Received 16 September 2017 • accepted 10 April 2018*)

Abstract−We studied particle deposition in rough channels, using the W-M fractal function to characterize a large-scale irregular surface with a root-mean-square roughness of 0.5 mm. The flow was numerically investigated by Reynolds stress model, and the particles were tracked by a Lagrangian particle model. An analysis of the flow field in a rough channel shows that the roughness enhances the max flow velocity and the pressure drop in the channel. It induces several eddies in the concave of the rough surface. We also compared particle deposition in a rough channel with particle deposition in a smooth channel. This comparison shows that the roughness significantly enhances the particle deposition of small particles, but the enhancement decreases with the increase of particle size. Moreover, the particle deposition ratio decreases with increasing flow velocity.

Keywords: Particle Deposition, Rough Channel, W-M Fractal Function, RSM Model, CFD

INTRODUCTION

The phenomenon of particle deposition widely exists in chemical, environmental and industrial applications [1], and it seriously affects the process of chemical reaction or heat transfer [2]. The engineering surface is not absolutely smooth, so some surface roughness can reach 0.5 mm [3], and have the properties of continuity, non-differentiability and self-affinity. Further, the roughness can potentially change both flow field and particle deposition [4]. So, it is meaningful to study the particle deposition in the rough channel.

Many studies about particle deposition on rough surfaces have been performed. Browne [5], El-Shobokshy and Ismail [6] and Wood [7] presented their own theories to calculate particle deposition on both smooth and rough surfaces, respectively. El-Shobokshy [8] experimentally studied the particle deposition on rough surfaces and compared results with the theory developed with Ismail [6], thereby confirming as accurate their earlier work for predicting the particle deposition on rough surfaces. Sommerfeld and Kussin [4,9] used phase Doppler anemometry (PDA) to experimentally study particle behavior in rough channel. They found that the wall roughness would broaden the particle velocity distribution. Over the past few decades, computational fluid dynamics (CFD) has grown considerably. Many numerical simulations have defined particle deposition in turbulent flow based on CFD [10-13]. The direct numerical simulation (DNS), large eddy simulation (LES) and Reynolds-averaged Navier-Stokes (RANS) model are core tools of CFD and have been widely used to study particle behavior and deposition in turbulent flow [14-17]. The RANS model has acceptable accuracy and consumes less computer resources; it is used by more and more researchers to predict the turbulent flow. Furthermore, the Reynolds stress model (RSM), as one of the RANS models, has been verified by Tian and Ahmadi [18] to simulate particle deposition in channel flow accurately. RSM can get more exact information about the turbulent flow than other RANS models because it considers the anisotropy of turbulence. Lain et al. [19] studied particle behavior in turbulent flow using an RSM to analyze their wall roughness model; likewise, their experimental results agreed with their model. Recently, Lu and Lu conducted a series of studies [20-23] about the particle deposition on regular rough surfaces using both the RSM and discrete particle model (DPM). They studied the effects of rib shapes, rib spacing and height, and rib arrangements on particle deposition.

However, the rough surfaces used by Lu and Lu [20-23] underwent numerical investigations of particle depositions arranged in much the same way as regular rough elements, such as square ribs or tri-angle ribs; thus, an information gap remained on how irregular rough elements affected particle deposition and distribution. With the development of fractal theory [24], some researchers began to build and define irregular rough surfaces based on the not so new (1975), but apparently neglected, fractal theory. Chen et al. [25] and Zhang et al. [26] used Cantor fractal structures to characterize rough surfaces, and studied the heat transfer in microchannels. The fractal Weierstrass-Mandelbrot (W-M) function was also used by Chen et al. [27,28] and Guo et al. [29] to build a rough surface in their respective microchannels. Furthermore, fractal geometry could be used to characterize engineering surfaces from micro to macro extents [30]. In summary, very little research has covered the deposition on large-scale irregular rough surfaces.

We adopted the W-M function to characterize the large-scale irregular rough surface. The turbulent flow in the channel was simulated by an RSM model, and the particle motion was tracked by the Lagrangian particle model. The particle deposition with a particle diameter from 3 μm to 40 μm and flow velocity from 3 m/s to 7 m/s was investigated here. Moreover, the different results obtained

†To whom correspondence should be addressed.
E-mail: wangx198911@163.com

while investigating the smooth and rough channels were used to define the effect of roughness on particle deposition.

PHYSICAL MODEL AND COMPUTATIONAL CASES

1. Fractal Characterization of Rough Surfaces

The engineered surfaces, such as the stainless-steel surfaces, have the properties of continuity, non-differentiability and self-affinity. They can be characterized by the W-M fractal function [31], and a surface roughness scale range that could be defined based on how many points were used to construct the rough surface and their size as measured from nanometers to millimeters according to diameter, length, and height [28]. The W-M fractal function can be expressed as

$$R(x)=G^{D-1}\sum_{n=n_1}^{\infty}\frac{\cos(2\pi\gamma^n x)}{\gamma^{(2-D)n}} \tag{1}$$

where G is a characteristic length scale, D is the fractal dimension, and γ is the scaling parameter; furthermore, n_1 is a parameter related to the sample length L_s, which is $\gamma^{n1}=1/L_s$ [27].

The root-mean-square (rms) roughness is defined as

$$\sigma=\sqrt{\frac{1}{Num}\sum_{i=1}^{Num}(R_i)^2} \tag{2}$$

where Num is the total number of points used to construct the rough surface, and R_i is the height of points, which can be calculated from Eq. (1). To get a rough surface where the root-mean-square roughness is equal to 0.5 mm, D is set as 1.2, G is set as 3.454×10^{-10} m and γ is set as 1.5.

2. Physical Model

Fig. 1 is a schematic of the rough-surface channel used in this paper. The length and height of channel is 150 mm and 20 mm, respectively. The upper wall and first 50 mm of the channel bottom is smooth; the last 100 mm of bottom is the rough surface established by the W-M function with the parameters defined in previous section.

Sixteen different computational cases were investigated and the detailed parameters of each case are shown in Table 1.

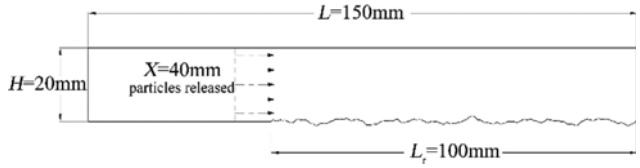

Fig. 1. Schematic of channel with rough surface.

Table 1. Computational cases

Case no.	Mean flow velocity (m/s)	Particle diameter (μm)	Surface type
1-6	5	3, 5, 10, 20, 30, 40	Smooth
7-11	3, 4, 5, 6, 7	10	Rough
12-16	5	3, 5, 20, 30, 40	Rough

NUMERICAL METHOD AND VALIDATION

1. Numerical Model

1-1. Continuous Phase

The fluid in the computational domain is considered incompressible since the flow velocity is low. Moreover, The RSM model was adopted to predict the turbulent flow. Thus, the governing equations are

mass equation

$$\frac{\partial\overline{u}_i}{\partial x_i}=0 \tag{3}$$

and momentum equation

$$\frac{\partial\overline{u}_i}{\partial t}+u_j\frac{\partial\overline{u}_i}{\partial x_j}=-\frac{1}{\rho}\frac{\partial\overline{p}}{\partial x_i}+\frac{1}{\rho}\frac{\partial}{\partial x_j}\left(\mu\frac{\partial\overline{u}_i}{\partial x_j}-\rho\overline{u_i'u_j'}\right) \tag{4}$$

where $\overline{u}_i$ is the time-average velocity, x_i is space position, t is time, $\overline{p}$ is time-averaged pressure, ρ is the constant air density, and μ is dynamic viscosity. The $\rho\overline{u'_iu'_j}$ is the Reynolds stress tensor.

The differential transport equation of the RSM model is presented as

$$\underbrace{\frac{\partial}{\partial t}(\overline{u_i'u_j'})+u_k\frac{\partial}{\partial x_k}(\overline{u_i'u_j'})}_{convective\ transport}=\underbrace{\frac{\partial}{\partial x_k}\left(\frac{v_t}{\sigma_k}\frac{\partial\overline{u_i'u_j'}}{\partial x_k}\right)}_{D_{T,ij}=diffusive\ transport}-\underbrace{\left(\overline{u_i'u_k'}\frac{\partial\overline{u}_j}{\partial x_k}+\overline{u_i'u_k'}\frac{\partial\overline{u}_i}{\partial x_k}\right)}_{P_{ij}=stress\ production}-\underbrace{C_1\frac{\varepsilon}{k}\left[\overline{u_i'u_j'}-\frac{2}{3}\delta_{ij}k\right]-C_2\left[P_{ij}-\frac{2}{3}\delta_{ij}P\right]}_{\phi_{ij}=pressure\ strain}-\underbrace{\frac{2}{3}\delta_{ij}\varepsilon}_{\varepsilon_{ij}=dissipation} \tag{5}$$

where the empirical constants are σ_k=1.0, C_1=1.8, and C_2=0.6 [32]. The turbulence dissipation rate, ε, is

$$\frac{\partial\varepsilon}{\partial t}+\overline{u}_j\frac{\partial\varepsilon}{\partial x_j}=\frac{\partial}{\partial x_j}\left[\left(\nu+\frac{\nu_t}{\sigma_\varepsilon}\right)\frac{\partial\varepsilon}{\partial x_j}\right]-C_{\varepsilon1}\frac{\varepsilon}{k}\overline{u_i'u_j'}\frac{\partial\overline{u}_i}{\partial x_j}-C_{\varepsilon2}\frac{\varepsilon^2}{k} \tag{6}$$

Here, the empirical constants are σ_ε=1.3, $C_{\varepsilon1}$=1.44 and $C_{\varepsilon2}$=1.92 [33].

1-2. Discrete Phase

As the particle concentration was sufficiently diluted in this study, the motion of particles was tracked by the Lagrangian approach. Moreover, the influence of particles on turbulent air flow was ignored and so was the interaction between particles. The governing equation of particle motion can be presented as,

$$m_p\frac{du_{pi}}{dt}=\frac{\pi d_p^2}{8}C_D\rho|u_i-u_{pi}|(u_i-u_{pi})+1.61(\mu\rho)^{1/2}d_p^2(u_i-u_{pi})\left|\frac{\partial u_i}{\partial x_i}\right|^{1/2}+m_p\frac{g_i(\rho_p-\rho)}{\rho_p} \tag{7}$$

Here, d_p is the diameter of particle, u_i is the fluid velocity and u_{Pi} is the particle velocity. ρ and ρ_p are the density of fluid and particle, respectively. Since $\rho_p\gg\rho$ here, the pressure gradient force and the virtual mass force were not taken into account. The three formulas on right side of Eq. (7) present the drag force, Saffman's lift force, and the resultant forces of gravity and buoyancy, respec-

tively. All particles were assumed to be solid spheres, and particle rotation was not considered, so the Magnus force was ignored. Since the particle diameter was much larger than 0.1 μm, Brownian diffusion was not considered.

C_D in Eq. (7) is the drag coefficient [34], and it is defined as

$$C_D=24/Re_p, \quad \text{for } Re_p<1 \tag{8}$$

and

$$C_D=24(1+0.15Re_P^{0.687})/Re_p, \quad \text{for } 1<Re_p<400 \tag{9}$$

Here Re_p is the particle Reynolds number, which can be calculated from

$$Re_p=\frac{\rho d_p|u-u_p|}{\mu} \tag{10}$$

1-3. Boundary Conditions and Solution Methods

To get the fully developed turbulent flow quickly, the 1/7th power law was employed in the inlet of channel. The velocity profile of inlet can be calculated from

$$U=U_{free}\left(\frac{y}{H/2}\right)^{1/7} \text{ for } y\le H/2 \tag{11}$$

$$U=U_{free}\left(\frac{H-y}{H/2}\right)^{1/7} \text{ for } y>H/2 \tag{12}$$

and

$$U_{free}=\frac{8}{7}U_{mean} \tag{13}$$

where the U_{mean} is the mean velocity of the channel cross section, and H is the channel height. The turbulence kinetic energy k is calculated as

$$k=\frac{\tau_w}{\rho_g\sqrt{C_\mu}}+\frac{y}{H/2}\left(0.002U_{free}^2-\frac{\tau_w}{\rho_g\sqrt{C_\mu}}\right) \text{ for } 0\le y\le H/2 \tag{14}$$

$$k=\frac{\tau_w}{\rho_g\sqrt{C_\mu}}+\frac{H-y}{H/2}\left(0.002U_{free}^2-\frac{\tau_w}{\rho_g\sqrt{C_\mu}}\right) \text{ for } H/2\le y\le H \tag{15}$$

and $$\tau_w=\frac{\rho U_{mean}^2}{2}\cdot f \tag{16}$$

Here, f is the fanning friction factor which can be calculated by,

$$f=0.0791\cdot Re^{-0.25}(2800<Re<10^5) \tag{17}$$

where the Reynolds number Re is computed by,

$$Re=\frac{U_{free}H\rho}{\mu} \tag{18}$$

The air dynamic viscosity μ is 1.789×10^{-5} kg·s/m. The air density is 1.225 kg/m^3.

The particle density is 2,000 times the density of air: 2,450 kg/m^3. The particles were released at the cross section of X=40 mm, where the air flow was fully developed. The total number of particles was 20000. Moreover, it was assumed that the initial velocity of the particle was the same as the average air velocity; and, the particle was deposited once it touched the bottom.

The governing equations of the continuous phase and discrete phase were solved by the finite volume method and the Runge-Kutta method, respectively. The convection terms and the diffusion terms of the continuous phase governing equations were discretized by the second-order upwind scheme and the central differencing scheme, respectively. The pressure and velocity fields were decoupled by the semi-implicit method for pressure linked equations (SIMPLE) algorithm.

2. Mesh and Model Validation

2-1. Grid Resolution

The hybrid grid technology was adopted to ensure the accuracy of the flow field information with fewer grids. The grids near the rough surface are unstructured meshes, and the other region contains structured meshes. Fig. 2 shows the local grids near the rough surface. Furthermore, the validation of grids-independent was made. The different test grid numbers for Case 3 were 271050, 481896, 589733 and 793138. The particle deposition ratio of the former 89 mm in channel was used as the monitoring parameter. The results are shown in Fig. 3; the calculation results with mesh number more than 481896 are almost consistent; therefore, the suitable grid number is 481896.

2-2. Model Validation

The air flow in smooth and rough channel was investigated to validate the correctness of the model used in this paper. The results

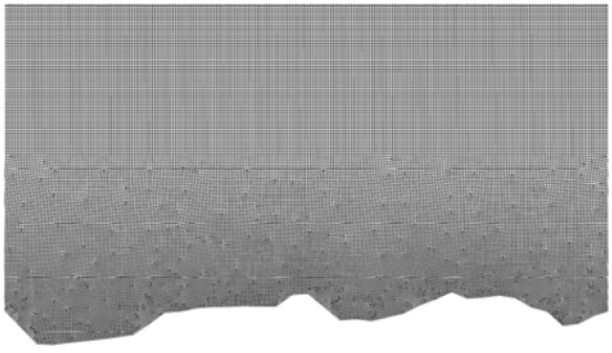

Fig. 2. Computational grids near the rough surface.

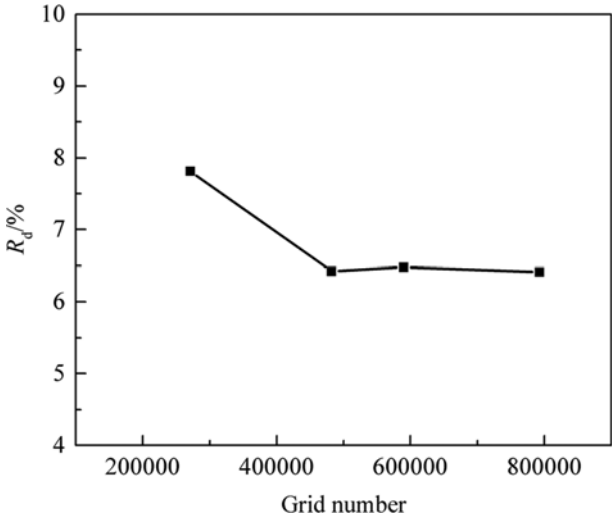

Fig. 3. Grid-independence check.

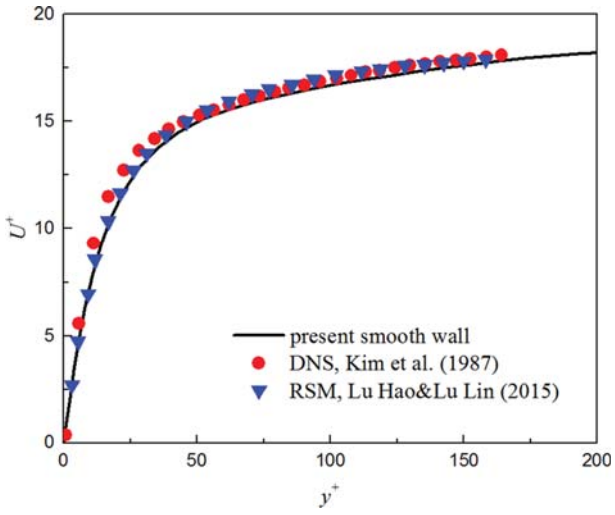

Fig. 4. Validation of flow velocity profiles in smooth channel.

of flow velocity in smooth channel where mean velocity equals 5 m/s were compared with previous studies, as shown in Fig. 4. The velocity profiles agree well with the DNS results by Kim et al. [35], and RSM results by Lu and Lu [20]. The average relative error η_{ave} between the present result and their value is 6.2% and 2.0%, respectively.

Here, y^+ is the dimensionless distance from the wall, and U^+ is the dimensionless velocity of air. They can be computed by,

$$U^+=u/u^+ \tag{19}$$

and

$$y^+=yu^*/\nu \tag{20}$$

where u is the velocity of air, u^* is the frictional velocity of air, y is the distance from the wall, and ν is the kinematic viscosity of air. The frictional velocity is defined as,

$$u^*=\sqrt{\tau_w/\rho}=U_{mean}\sqrt{f/2} \tag{21}$$

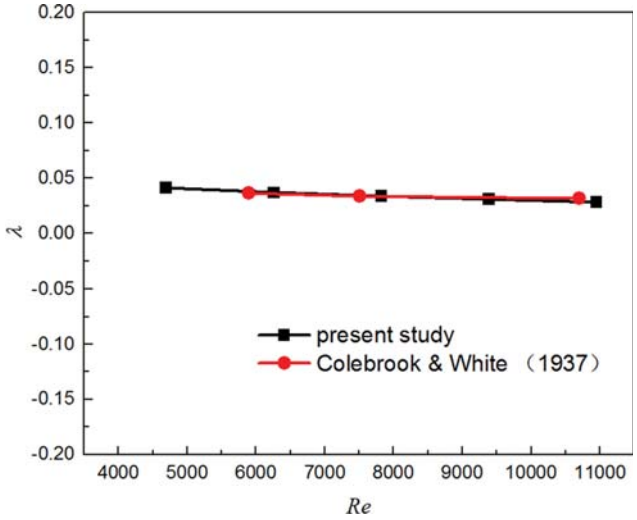

Fig. 5. Validation of resistance coefficient λ evolution according to Re.

And the average relative error η_{ave} can be computed by,

$$\eta_{ave}=\frac{1}{n}\sum_{i=1}^{n}\frac{|v_i-\hat{v}_i|}{v_i} \tag{22}$$

where v_i is the simulation value in this paper and $\hat{v}_i$ is the value of previous studies.

The result of flow in rough channel is validated by comparing the results presented here with the experimental data by Colebrook and White [36], as shown in Fig. 5. The resistance coefficient λ between our results and their results is very consistent, and the average relative error η_{ave} is 3.2%.

The resistance coefficient λ can be calculated from

$$\lambda=\frac{8\tau_w}{\rho U_{free}^2} \tag{23}$$

COMPUTATION OF PARTICLE DEPOSITION VELOCITY AND RATIO

The non-dimensional deposition velocity V_d^+ was adopted to present the results of deposition calculations. Moreover, V_d^+ is always versus non-dimensional particle relaxation time τ^+ to form curves [37]. The non-dimensional deposition velocity is defined as,

$$V_d^+=V_d/u^* \tag{24}$$

where the V_d is the deposition velocity of particles. Liu and Zhang [38] derived an equation to calculate deposition velocity. Here, an equation was derived by the same method, given as

$$V_d=\frac{HU_{mean}\ln(1-N_{dep}/N_{in})}{L} \tag{25}$$

where N_{dep} is the number of particles which are deposited on the surface, and N_{in} is the number of incoming particles.

The non-dimensional particle relaxation time is written as,

$$\tau^+=\frac{Sd_p^2u^{*2}}{18\nu^2}C_c \tag{26}$$

S is the particle-to-gas density ratio. C_c is the Cunningham slip correction factor [39] and can be given as,

$$C_c=1+\frac{2\lambda_g}{d_p}[1.257+0.4e^{-(1.1d_p/(2\lambda_g))}] \tag{27}$$

where λ_g is the gas molecular mean free path.

To observe the particle deposition for different cases more clearly, a deposition ratio R_d is defined as

$$R_d=\frac{N_d}{N_t}\times 100\% \tag{28}$$

where N_d is the number of deposited particles on surface, and N_t is the number of particles that transited through the section upon the deposit surface.

RESULTS AND DISCUSSION

1. Flow Field

The turbulent air flow fields of smooth and rough channel were

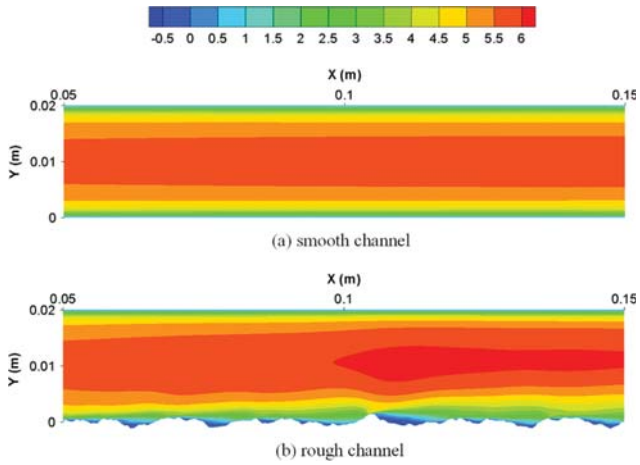

Fig. 6. Velocity fields of smooth and rough surface (U_{mean}=5 m/s).

compared, as shown in Fig. 6. From Fig. 6(b), the rough surface disturbs the flow field compared to the smooth channel and makes the flow field more complex. Moreover, it makes the upper boundary layer thinner and increases the bottom boundary layer thickness. The rough surface increases the max flow velocity and the average flow velocity of the channel by 6.5% and 7.3%, respectively.

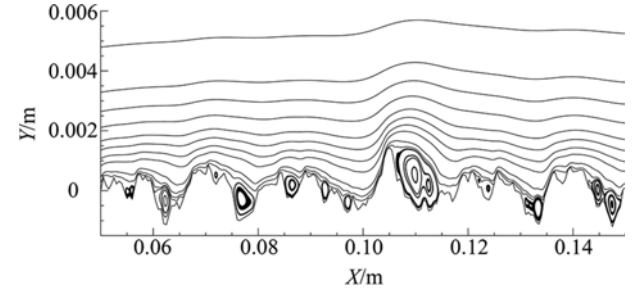

Fig. 7. Streamlines near the rough surface (U_{mean}=5 m/s).

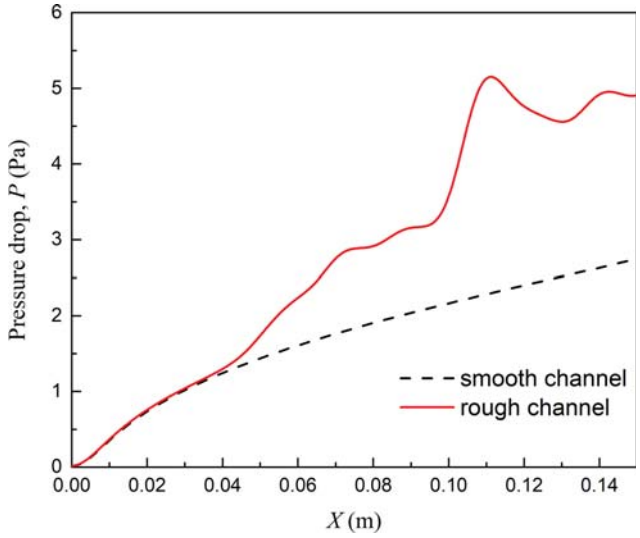

Fig. 8. Pressure drop of air flow in smooth and rough channels (U_{mean}= 5 m/s).

As shown in Fig. 7, several eddies appear at the concave regions. And, the size of the eddy is related to the steepness of the peaks and valleys. The largest eddy appears at the steepest peak-valley, 0.105-0.115 m, in the present study. The pressure drop in the rough channel is compared with the smooth channel in Fig. 8. Roughness makes the whole pressure drop increase. From Fig. 7 and Fig. 8, the pressure drop fluctuates with the undulation of the rough surface. At the rough peak, as the diameter of the channel becomes smaller, the velocity of the section increases and the pressure decreases. At the rough valley, the diameter of the channel becomes bigger, the velocity of section decreases, and the pressure increases. Therefore, the maximum value of the pressure drop also occurs in the region of 0.105-0.115 m, and, it is about 2.3-times greater as the pressure drop in the same location of the smooth channel.

2. Particle Deposition

The results of particle deposition on smooth channel surfaces were analyzed. The curve of non-dimensional deposition velocity versus non-dimensional particle relaxation time is shown in Fig. 9. Moreover, the results were compared with previous studies [40-42]. The prediction of particle deposition in this paper agrees well with the previous study and once again verifies the accuracy of the model used herein. Wood [7] determined that the particle deposition on a smooth surface can be divided into three regions. For $\tau^+ \lesssim 10^{-1}$, the Brownian and turbulent eddy diffusion are the main effect on particle deposition since the particle is very fine; it is turbulent particle diffusion regime. And, the V_d^+ decreases with the increase of τ^+. For $10^{-1} \lesssim \tau^+ \lesssim 10$, the turbulent eddy and particle inertia are the main reason for particle deposition; it is an eddy diffusion-impaction regime. V_d^+ increases with the increase of τ^+. For $\tau^+ \gtrsim 10$, as the particle is larger, particle deposition is mainly affected by the particle inertia; it is inertia-moderated regime. The V_d^+ keeps almost a constant value with the increase of τ^+. This steady value has been accepted and referred to by many researchers [20,43]. The scope of this study consists of only two regions: the eddy diffusion-impaction regime and the inertia-moderated

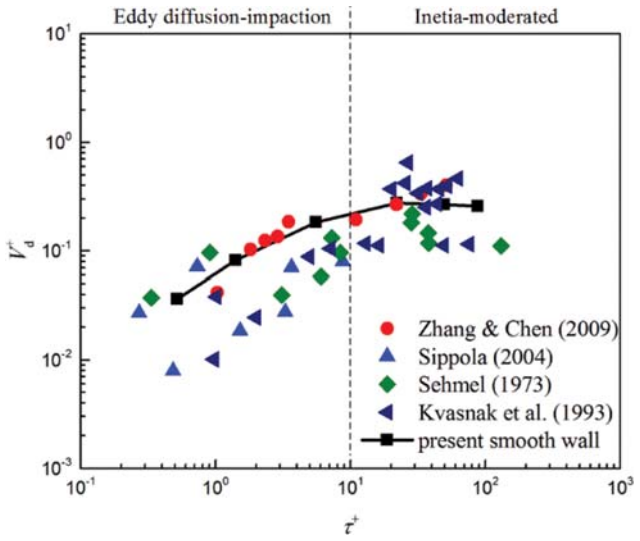

Fig. 9. Particle deposition in smooth channel.

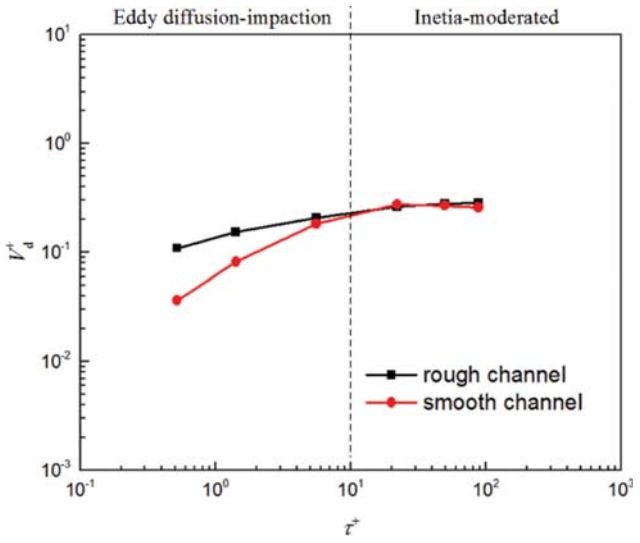

Fig. 10. Comparison of deposition in rough channel and smooth channel.

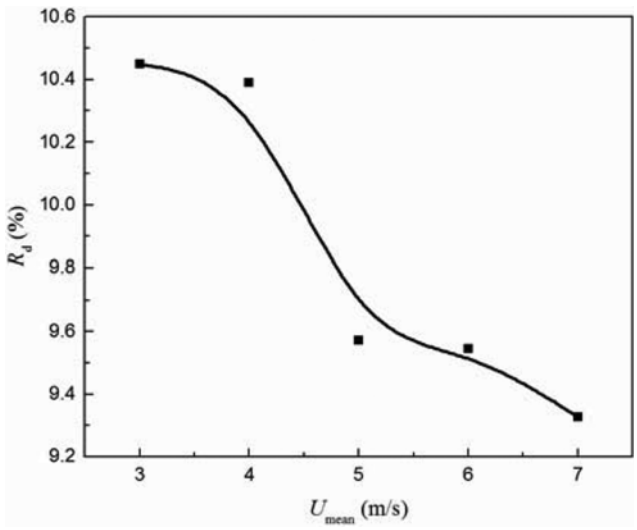

Fig. 12. Particle deposition ratio with different U_{mean} in rough channel (d_p=10 μm).

regime. The trends in this study are also consistent with the law in each of these regions.

Fig. 10 compares the deposition in a rough channel with a smooth channel. The graph shows that the roughness increases the V_d^+ compared with the smooth channel. Especially in the eddy diffusion-impaction region, the V_d^+ in rough channel is significantly larger than that in smooth channel. However, in the inertia-moderated region, the increase is not remarkable, and the V_d^+ is almost not increased. The reason for the enhancement of V_d^+ on the rough surface when τ^+ is small is that the roughness engenders many eddies as shown in Fig. 7. Furthermore, the turbulent eddy is the main reason for particle deposition in the eddy diffusion-impaction region when τ^+ is small. With the increase of τ^+, which means that the diameter of particles becomes larger and the mass of particle also become larger, the effect of particle inertia becomes greater and the effect of the turbulent eddy becomes relatively smaller. The effect of roughness on the particle deposition also becomes relatively smaller. These effects cause the decrease of enhancement in V_d^+ with the increase of τ^+. When the τ^+ reaches 10, particle inertia is the main mechanism of particle deposition, and the effect of eddies, which are created by the roughness is slight; meanwhile, almost no enhancement of V_d^+ occurs in the rough channel compared with the V_d^+ development in the smooth channel.

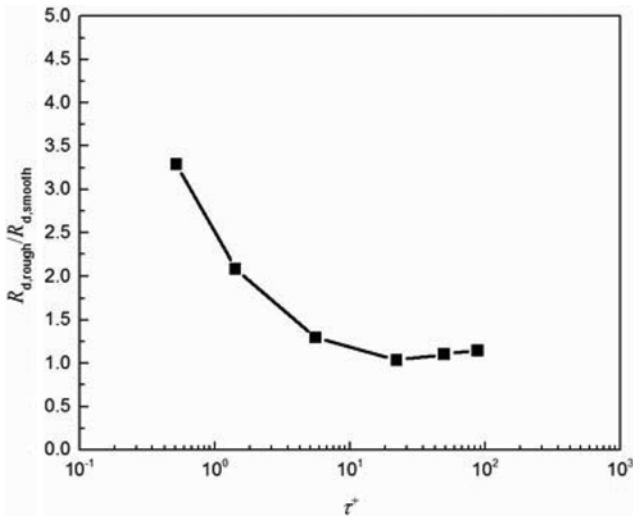

Fig. 11. Particle deposition enhancement by roughness.

To show the effect of roughness on particle deposition more intuitively, the enhancement of deposition ratio was analyzed as shown in Fig. 11. The maximum enhancement of the deposition ratio can become 3.3-times in the range of this study. Additionally, the enhancement decreases with the increase of τ^+, but it reaches the minimum when τ^+ near 10, after which the deposition becomes steady at last.

The particle deposition ratio with different mean air flow velocity is shown in Fig. 12. It decreases with the increase of flow velocity, because the increase in air velocity makes the residence time of particles in the channel shorter, resulting in a decrease in deposition ratio.

CONCLUSIONS AND REMARKS

The W-M function was introduced to characterize large-scale irregular roughness. The particle deposition in a rough channel was numerically investigated by RSM with a Lagrangian approach. The effect of roughness on flow fields and particle deposition velocities was analyzed. Enhancement of particle deposition ratio by roughness was discussed. The conclusions follow:

(1) Roughness makes the air flow more complex, and increases the thickness of the boundary layer. Eddies often appear at the concave regions. All of the velocity and pressure drop activities are enhanced by roughness. The pressure drop fluctuates with undulation of the rough surface.

(2) The roughness enhances the deposition velocity, especially for the small particles. The main reason for the enhancement is the

eddy created by the rough surface. And the enhancement of deposition velocity decreases with the increase of τ^+.

(3) The deposition ratio in a rough channel is enhanced compared with that in a smooth channel. However, with the increase of τ^+, the enhancement becomes slight. Finally, the deposition ratio decreases with flow velocity.

Preliminary results show that the large-scale irregular roughness can significantly influence the flow field in the near wall region and enhance the deposition velocity of small particles with $\tau^+<1$. However, due to the limitation of method and two-dimensional (2D) physical model used in this paper, the particle resuspension and the effect of second secondary flow cannot be simulated. Related experiments and three-dimensional (3D) simulation need to be carried out in the future.

ACKNOWLEDGEMENT

This study was funded by the National Natural Science Foundation of China (No. 51776032).

NOMENCLATURE

C_c : cunningham slip correction factor
C_D : drag coefficient
D : fractal dimension
f : fanning friction factor
G : characteristic length scale
H : channel hight [m]
k : turbulence kinetic energy [m^2/s^2]
L : the length of channel [m]
L_s : the sample length [m]
N_{dep} : particle deposition numbers to wall
N_{in} : incoming particle numbers
N_d : the number of deposited particles on surface
N_t : the number of particles that transited through the section upon the deposit surface
R_d : particle deposition ratio
Re : Reynolds number
Re_p : particle Reynolds number
S : ratio of particle-to-fluid density
U_{mean} : mean velocity of air [m/s]
U_{free} : freestream velocity of air [m/s]
u : velocity of fluid [m/s]
u_p : velocity of particle [m/s]
u^* : frictional velocity of air [m/s]
v_i : simulation value
$\hat{v}_i$: value of previous studies
V_d^+ : non-dimensional deposition velocity
V_d : particle deposition velocity [m/s]

Greek Symbols

ε : turbulence dissipation rate [J/(kg·s)]
μ : dynamic viscosity of air [Pa·s]
ρ : air density [kg/m^3]
ρ_p : particle density [kg/m^3]
ν : kinetic viscosity of air [m^2/s]
τ_w : shear stress on the wall [Pa]
τ^+ : non-dimensional particle relaxation time
γ : scaling parameter
σ : root-mean-square roughness [m]
η_{ave} : average relative error
λ : resistance coefficient
λ_g : gas molecular mean free path [m]

REFERENCES

1. G. Lecrivain, L. Barry and U. Hampel, *Powder Technol.*, **258**, 134 (2014).
2. H. Feng, C. Wang and Y. Huang, *Korean J. Chem. Eng.*, **34**, 2832 (2017).
3. A. C. K. Lai, M. A. Byrne and A. J. H. Goddard, *J. Aerosol Sci.*, **32**, 121 (2001).
4. M. Sommerfeld and J. Kussin, *Powder Technol.*, **142**, 180 (2004).
5. L. W. B. Browne, *Atmospheric Environment (1967)*, **8**, 801 (1974).
6. M. S. El-Shobokshy and I. A. Ismail, *Atmospheric Environment (1967)*, **14**, 297 (1980).
7. N. B. Wood, *J. Aerosol Sci.*, **12**, 275 (1981).
8. M. S. El-Shobokshy, *Atmos. Environ.*, **17**, 639 (1983).
9. J. Kussin and M. Sommerfeld, *Exp. Fluids*, **33**, 143 (2002).
10. Q. Chen, *Build. Environ.*, **44**, 848 (2009).
11. H. Jiang, L. Lu and K. Sun, *Build. Environ.*, **45**, 1184 (2010).
12. K. Sun, L. Lu and H. Jiang, *Build. Environ.*, **46**, 1251 (2011).
13. S. Andarwa and H. B. Tabrizi, *Korean J. Chem. Eng.*, **34**, 1319 (2017).
14. M. De Marchis, B. Milici, G. Sardina and E. Napoli, *Int. J. Multiphase Flow*, **78**, 117 (2016).
15. B. Milici and M. De Marchis, *Int. J. Heat Fluid Flow*, **60**, 1 (2016).
16. J. Yao and M. Fairweather, *Chem. Eng. Sci.*, **84**, 781 (2012).
17. G. Lecrivain, D.-M. Sevan, B. Thomas and U. Hampel, *Adv. Powder Technol.*, **25**, 310 (2014).
18. L. Tian and G. Ahmadi, *J. Aerosol Sci.*, **38**, 377 (2007).
19. S. Laín, M. Sommerfeld and J. Kussin, *Int. J. Heat Fluid Flow*, **23**, 647 (2002).
20. H. Lu and L. Lu, *Build. Environ.*, **85**, 61 (2015).
21. H. Lu and L. Lu, *Build. Environ.*, **92**, 317 (2015).
22. H. Lu and L. Lu, *Build. Environ.*, **94**, 43 (2015).
23. H. Lu and L. Lu, *Appl. Therm. Eng.*, **93**, 697 (2016).
24. B. B. Mandelbrot, *Fractals: Form, chance and dimension*, W. H. Freeman & Co., San Francisco (1977).
25. Y. Chen, P. Fu, C. Zhang and M. Shi, *Int. J. Heat Fluid Flow*, **31**, 622 (2010).
26. C. Zhang, Z. Deng and Y. Chen, *Int. J. Heat Mass Transfer*, **70**, 322 (2014).
27. Y. Chen, C. Zhang, M. Shi and G. P. Peterson, *Phys. Rev. E Stat. Nonlin. Soft Matter Phys.*, **80**, 026301 (2009).
28. Y. Chen, C. Zhang, M. Shi and G. P. Peterson, *Appl. Phys. Lett.*, **97**, 084101 (2010).
29. L. Guo, H. Xu and L. Gong, *Appl. Therm. Eng.*, **84**, 399 (2015).
30. F. F. Ling, *Wear*, **136**, 141 (1990).
31. A. Majumdar and C. L. Tien, *Wear*, **136**, 313 (1990).
32. B. E. Launder, G. J. Reece and W. Rodi, *J. Fluid Mech.*, **68**, 537 (1975).
33. B. E. Launder and D. B. Spalding, *Lectures in mathematical models*

of turbulence, Academic Press, London (1972).
34. W. C. Hinds, *Aerosol technology: Properties, behavior, and measurement of airborne particles*, Wiley, New York (1984).
35. J. Kim, P. Moin and R. Moser, *J. Fluid Mech.*, **177**, 133 (1987).
36. C. F. Colebrook and C. M. White, *Proceedings of the Royal Society A: Mathematical, Physical and Engineering Sciences*, **161**, 367 (1937).
37. A. Guha, *J. Aerosol Sci.*, **28**, 1517 (1997).
38. H. Liu and L. Zhang, *Appl. Therm. Eng.*, **31**, 3402 (2011).
39. H. Ounis and G. Ahmadi, *J. Fluids Eng.*, **112**, 114 (1990).
40. W. Kvasnak, G. Ahmadi, R. Bayer and M. Gaynes, *J. Aerosol Sci.*, **24**, 795 (1993).
41. M. R. Sippola and W. W. Nazaroff, *Aerosol Sci. Technol.*, **38**, 914 (2004).
42. Z. Zhang and Q. Chen, *Atmos. Environ.*, **43**, 319 (2009).
43. N. Gao, J. Niu, Q. He, T. Zhu and J. Wu, *Build. Environ.*, **48**, 206 (2012).